5/12/95, 3:22 PM

LA-UR-95-317

An experimental study of the flow after shock interactions with cylindrical helium inhomegeneities.

By J. M. Budzinski, E. E. Zukoski,
AND F. E. Marble

An experimental study of the flow after shock interactions with cylindrical helium inhomegeneities.

By J. M. Budzinski*, E. E. Zukoski, AND F. E. Marble

California Institute of Technology,
Pasadena, CA 91125, USA

A shock traveling in air interacts with a laminar jet of helium flowing normal to the direction of shock propagation. Planar laser Rayleigh scattering is used to study the deformation and motion of the originally circular jet cross-section. The velocity of the jet before the shock interaction is much less than the velocities generated by the shock wave. Thus, the helium jet serves to create a cylindrical bubble of a lighter density gas imbedded in a heavier one. Four different shock Mach numbers (1.066, 1.14, 1.5, and 2.0) are studied. Two different jet/air density ratios are examined by using pure helium in the jet in one case, and a mixture of air/helium in the other. After the shock interaction, a vortex pair forms from the baroclinically generated vorticity. The experiments measure the velocity of the helium relative to the surrounding air, the spacing between the vortex cores, and the circulation of the vortices. Experiments viewing the reflected shock interaction are also performed. Excellent agreement is found with previous computational studies.

* Currently Technical Staff Member, Los Alamos National Laboratory.

1. Introduction

This study is concerned with the unsteady, two-dimensional interaction of a shock wave(s) with a cylindrical region of lower density fluid surrounded by a heavier one. Here, a planar shock travels normal to the cylinder axis. This interaction is an example of the shock-induced Rayleigh-Taylor instability, or Richtmyer-Meshkov instability (Richtmyer 1960, Meshkov 1969). The focus of this paper is the distortion and motion of the lighter fluid after interactions with an initial and a reflected shock. Shock interactions with density inhomogeneities have many applications in engineering and science, ranging from hypersonic propulsion to inertial confinement fusion.

Rudinger & Somers (1960) were the first to study this problem in order to simulate how well

tracer particles follow fluid flows. More recently Haas & Sturtevant (1987) studied the interaction of weak shocks with discrete interface cylindrical volumes confined by microfilm membranes. Picone & Boris (1987) and Marble *et al.* (1987) numerically simulated the experiments of Haas & Sturtevant. Jacobs (1992) started the current experimental program by creating diffuse interface cylindrical volumes with laminar jets of helium inside a shock tube. He viewed a two dimensional cross section of the flow field with the planar laser induced fluorescence of a tracer dye (biacetyl) premixed with the helium. Yang (1991, 1994b) performed the most comprehensive simulations to date of shock interactions with diffuse interface cylindrical volumes. Samtaney & Zabusky (1994) used a shock polar analysis and direct numerical simulations to studied shock interactions with heavy gas, discrete interface, cylinders.

These studies have contributed to a fundamental understanding of the general flow characteristics, and have developed scaling laws for the generation of vorticity during the shock interaction. They have shown that the vorticity generated at the boundaries of the cylindrical volume causes a stream of air to divide the initial circular cross section into two lobes. Each lobe is further divided into a tail region and a vortex core. The cores combine to form a vortex pair which moves relative to the surrounding fluid.

Most of the above studies, however, were limited to relatively weak shock waves, and have only studied the incident shock interaction. Only the computational and analytic work by Yang (1991, 1994b) includes a broad range of incident Mach numbers and reflected shock interactions.

Here, we present the results of experiments in a shock tube, which cover a wide range of incident shock Mach numbers, different density ratios between the jet and surrounding fluid, and reflected shock interactions. The density ratio between the gases can be characterized by the Atwood number (A) defined as:

$$A = \frac{\rho_h - \rho_l}{\rho_h + \rho_l}$$

where ρ_l and ρ_h are the densities of the light and heavy gas. Four different Mach numbers (1.066, 1.14, 1.50 and 2.00), and two different Atwood Numbers (0.66 and 0.22) were studied. Reflected shock experiments were performed for all but the

Mach 1.50 case. We visualize the deformation of the jet cross section with a planar laser Rayleigh scattering technique, which enables more precise and accurate measurements than the techniques using a tracer gas. The current measurements of the vortex pair velocities, spacing and circulation, are compared to those of the previous studies. Some of the discrepencies that existed in the previous studies are clarified. Estimates of the molecular mixing induced by the shock interaction are presented elsewhere (Budzinski *et al.* 1995).

2. Experimental Apparatus

2.1 GALCIT 17" shock tube and test sections

A cylindrical inhomogeneity of helium surrounded by air is created by injecting a laminar jet of helium inside the GALCIT 17-inch shock tube (Liepmann *et al.* 1962); a side view of the apparatus is shown in Figure 1. The jet flows vertically upward into the test section and normal to the direction of the shock propagation.

Two 2-ft long test sections with square cross sections 10.5 inches on a side can be attached in series to the end of the tube. Each section has a pair of 6"diameter windows on opposite side walls. For the Rayleigh scattering experiments, the test sections are oriented with one window on the bottom so the jet can be visualized from below. A back end plate, also with a 6 inch window, closes the tube.

After interacting with the helium jet, the shock wave continues down the shock tube and reflects off the end plate. With both test sections in place the distorted helium jet translates past the window before an interaction with the reflected shock occurs. To view the reflected shock interaction, we remove the second test section and shorten the distance between the jet and the end wall to 11.75 inches. For the Mach 2.0 case, an additional plate is offset 5" from the end wall.

For stronger shock experiments, the shock tube is pumped down below atmospheric pressures. Otherwise, the pressures generated would compromise the structural integrity of various shock tube components. For Mach numbers of 2.0, 1.50, 1.14, and 1.066 the initial pressures are 0.08, 0.23, 0.55 and 1.0 atmospheres respectively.

2.2 Planar Laser Rayleigh Scattering System

The primary diagnostic used in the experiments is Planar laser Rayleigh scattering. A flash-lamp pumped dye laser generates a 4 J, 700 nsec long laser beam pulse at 480 nm. Cylindrical lenses transform this beam into a thin sheet of light, less than 1.5 mm thick at the focus. The sheet intersects a cross section of the deforming helium jet at about 5 nozzle exit diameters above the nozzle exit. The Rayleigh scattered laser light from the gas molecules generates an image in the plane of the laser sheet that is captured by a cooled CCD camera. In the picture, the air is bright and the helium is dark.

Thus, the technique measures two-dimensional cross section of the flow in a clear and unambiguous way. No tracer gases are required, so the pictures are not affected by the differential diffusion. The low noise camera, together with the high energy laser, produce exceptional Rayleigh scattering images.

The CCD has an array of 576 by 384 square pixels each 20 microns on a side. In the plane of the laser sheet, 16 pixels view about 1 mm. Thus, the camera provides fine resolution of detailed structures, especially of those generated in the reflected shock experiments. Only one picture is taken each time the shock tube is fired; a sequence is built by performing multiple experiments.

A calibration procedure is used to remove all important intensity variations that are not associated with the local helium concentration. The procedure compensates for the shot to shot laser sheet variation, the background illumination, variations due to the camera optics, and the pixel to pixel variations in the CCD. Only minor variations due to the interaction of the laser light with helium are not accounted for. Helium gradients cause small index of refraction gradients, which slightly refract the laser sheet as it travels from right to left through the jet cross section. This effect is visible as subtle horizontal streaks on the left side of some of the pictures. This is the same mechanism that creates shadowgraph and scheleirn pictures.

The initial pressure also affects the quality of the scattering signal. As the initial pressure is lowered, the number density of molecules after the shock interaction decreases, and the signal to noise ratio increases in the pictures. Hence the Mach 2.0 pictures look 'grainier' than the Mach 1.066 pictures.

2.3 Characteristics of the laminar helium jet

The nozzle of the helium jet is a brass tube with an I.D. of 0.305 inches (0.D. of 3/8") that extends two inches into the test section through the bottom wall. Contamination of the test section with helium is prevented by exhausting the jet through a 9/16" diameter exit orifice located above the nozzle, and flush with the upper wall of test section. A Welsh vacuum pump is connected to the exhaust.

Previous investigations (Jacobs 1992 and Budzinski 1992) have used spark shadowgraphy to view the interaction from the side. They showed

that the flow field produced with this method is two-dimensional after the shock interaction.

Studies are made of the two-dimensional cross section of the deforming helium jet at about 5 nozzle exit diameters above the nozzle exit. This far above the nozzle exit the jet boundary is diffuse, and the molar composition of the jet on its centerline is about 92% helium and 8% air. The lower Atwood number case uses a mixture of 50% air and 50% helium (molar concentrations) at the nozzle exit. This corresponded to 57% air and 43% helium in the plane of the laser sheet.

For the cases with the jet initially at one atmosphere, the jet has a helium volumetric flow of 60 cm^3/sec. This results in an average velocity of 130 cm/sec at the exit and a Reynolds number of 75 based on the average velocity, the jet diameter, and the kinematic viscosity of helium. For the cases where the initial pressure is below atmospheric in the test sections, the jet Reynolds number was kept constant by keeping the helium mass flow rate the same. At the different initial pressures, the jet has slightly different properties. For pressures of 1 atm, 0.55 atm, 0.23 atm, and 0.08 atm, the initial jet radii (based on the contour representing 50% of the centerline helium concentration) are 0.45, 0.55, 0.62, and 0.63 cm respectively.

2.4 Timing, Control, and Data Acquisition

The main shock tube and the test sections are each fitted with two piezoelectric pressure transducers, which allow the shock velocity and Mach number to be measured. Experiments were performed which compared Mach numbers based on the timing measurements with those based on the density jump across the shock and measured with the Rayleigh scattering diagnostic. This comparison indicated the timing measurements consistently err by about 0.5%. This difference is attributed to errors in the measured distance between the transducers, and in a difference from the speed of sound found from the ideal gas relations. For the majority of experiments the Mach number is found by applying the 0.5% correction to the timing measurements. The transducers are also used to trigger a Stanford Research System model DG535 digital delay/pulse generator which controlled the timing of the data acquisition systems.

Two computers are used to acquire and store

the data from the experiments. The output of the pressure transducers is recorded on an RC Electronics Model ISC-67 Computerscope board installed in an IBM model AT computer. The Rayleigh scattering images are transferred to and stored on a 386/33 AT compatible computer.

A more detailed description of operation is given in Ref. [19-23]

3. Results and Discussion

3.1 Flow Visualization

3.1.1 Motion after the Incident Shock Interaction

Figure 2 through Figure 6 display the Rayleigh scattering pictures of the deforming helium jet for the different Mach, and Atwood numbers studied. The shock wave travels from left to right in the pictures. For display purposes, the pictures were smoothed by averaging over 3 pixel by 3 pixel boxes. The times given for each picture are normalized by a developmental time scale τ. For weak waves, Marble (1990) suggested $\tau = r_1^2/\Gamma$, where Γ is the circulation generated by the shock, and r_1 is the initial jet radius. Yang (1994b) modified this timescale for stronger shocks, and using his model for the circulation the time scale can be rewritten in the form:

$$\tau = \frac{r_1}{4A\Delta u},$$

where Δu is the change in velocity across the shock traveling in the ambient gas.

The qualitative features after the first shock interaction are very similar to those found in previous investigations (Haas & Sturtevant 1988, Picone & Boris 1988, Jacobs 1992, Yang 1994b). The initially circular cross-section is first divided into an upper and lower lobe. Then a vortex pair and tail regions form.

The deformation and motion of the cross section can be explained in terms of vortex dynamics. The two dimensional vorticity equation is

$$\frac{D(\omega/\rho)}{Dt} = \frac{1}{\rho^3}\nabla\rho \times \nabla P,$$

where ω is the vorticity, ρ is the density, and P is the pressure. As the incident shock passes over the helium jet, vorticity is baroclinically generated where the density gradients of the jet are not parallel to the pressure gradients of the shock. This vorticity is created on the edge of the jet with counter clockwise vorticity on the top half of the cross section (above the symmetry line) and clockwise vorticity on the bottom (below the symmetry line).

The simulations of Picone & Boris (1988) indicate that the particle paths of the vorticity on the upper and lower halves of the cross section, are similar to inward spirals, which lead to the formation of a vortex pair. Figure 7 shows the path of the vorticity which was generated near the top and bottom edges of the initially circular cross-section. The vorticity on the top edge of the cross section, first moves upstream, then toward the symmetry line, and then downstream. The vorticity on the

bottom follows a similar path. This motion divides the cross section into the upper and lower lobes. As the spiral motion continues, the vorticity proceeds to move slightly away from the symmetry line, and slightly upstream as the vortex cores are formed. This doubling back in the upstream direction pinches off and creates the tail regions.

Qualitatively, the vorticity equation can be used to understand the effect of changing the shock Mach number and gas density ratio. As the shock Mach number increases, there are two major changes in the vorticity distribution. First, the magnitude of the vorticity increases with the increasing pressure ratio of the shock. Second the vorticity distribution becomes more compressed in the shock direction. Consequently, for low Mach numbers the jet boundary (where the vorticity is generated) is nearly circular just after the shock interaction. However, for higher Mach numbers, the vorticity lies on an elliptic contour since the jet cross-section is compressed mostly in the direction of the shock propagation. On the other hand, as the Atwood number increases, the single most important change in the vorticity distribution is an increase in its magnitude.

Figure 2 through Figure 6 show that the size of the tail regions becomes smaller as the shock Mach number increases. Yet, as the Atwood number is changed, the tail sizes remain nearly the same. Consequently, the changes of tail size are most likely due to the changing aspect ratio of the elliptical vorticity distribution that exists just after the shock interaction. As the Mach number increases, the vorticity generated on the upstream and downstream sides of the cross section, just after the shock interaction, lie closer together. As the vorticity spirals to form vortex cores, it does not move as far in the upstream or downstream directions, and is not capable of doubling back and pinching off as large of a tail region.

The aspect ratio of the elliptic vorticity distribution just after the shock interaction, can also be changed by modifying the initial jet geometry. Yang (1991) simulated shock interactions with elliptic cross section jets. Here also, the tail regions became progressively smaller as the aspect ratio between the horizontal, and vertical axis was decreased.

3.1.2 Motion After the Reflected Shock Interaction.

Figure 2, Figure 3, Figure 5, and Figure 6 include pictures after reflected shock interactions. These pictures agree very well with the simulations of Yang (1991, 1994b). For incident Mach numbers of 1.066, 1.14, and 2.0, the reflected shock Mach numbers are calculated from basic 1-D gasdynamcis to be 1.065, 1.134 and 1.73 respectively.

The vorticity generated by the reflected shock splits each vortex core into two regions of vorticity: one that is closer to the symmetry line (inner vortex), and one that is further from the symmetry line (outer vortex). Each inner vortex has the same sign as it's parent, pre-reflected shock vortex. Each outer vortex has the opposite sign as its respective parent vortex. Since the vorticity that was present before the reflected shock, adds to the inner vorticity, and partly negates the outer, the magnitude of the circulation for the inner vortices is larger than that of the outer ones.

This new vorticity distribution further deforms the helium cross-section. The Rayleigh scattering pictures show that the inner vortices induce the weaker outer ones to rotate upstream and then toward the symmetry line. This divides the helium that was in the pre-reflected shock, vortex cores. Simultaneously the outer vortices induce the inner ones toward the symmetry line. Both motions tend to move the helium closer to the symmetry line.

The reflected shock interaction also generates vorticity in the tail regions. This is more pronounced in the lower Mach number interactions, (1.066, 1.14) where the tails are horizontal and contain more helium mass. Since the tails contained little vorticity before the reflected shock interaction, nearly equal and opposite circulation is generated on their tops and bottoms. Visible vortex pairs form from the tail regions.

There are noticeable differences between the reflected shock interactions with relatively weak waves (1.066, 1.14), and the reflected shock interaction generated by a Mach 2.0 incident shock. For the Mach 2.0 case, the tails are nearly vertical near their left tip and become horizontal only where they attach to the vortex cores. The density gradients in the tails are also smaller. As a result, proportionally less vorticity is generated in the tail regions for the Mach 2.0 case. Figure 5 shows that this vorticity can not escape the strong inner vortices and is rotated around their cores. The vorticity

generated in the tail regions shows up as minor bumps on the tail strand just upstream of the vortex cores in Figure 5i. This vorticity is then rotated downstream and can be seen in Figure 5j just to the right of the strong inner vortex cores.

The Rayleigh scattering diagnostic also reveals interesting features of the shock dynamics during the reflected shock interaction in Figure 5h&i. The reflected shock becomes curved as it travels through the vortex centers due to two effects; first the induced velocity of the vortices impedes the progression of the shock wave between the cores, while increasing the wave speed above and below the vortices. Second, the higher speed of sound of helium allows the shock wave to move faster through the cores than outside of them. The curved surfaces lead to the formation of sharp corners and the development of two triple-point intersections visible in Figure 5i. The triple-point intersections generate slip lines that can be seen in Figure 5i,j and k.

3.2 Quantitative Measures of the Motion of the Vortex Pairs

Figure 8 displays the position of the center of helium mass vs. time for all the experiments performed. Since the experiments are nearly repeatable, the points only have small random deviations from a straight line fit through each series. For a Mach number of 1.14, less circulation is generated for the case with the lower Atwood number, and the center of mass travels slightly slower. The ~~Figure~~ data also shows that the reflected shock does not completely halt the forward motion of the helium.

The spacing between the vortex cores is modeled by finding the regions of highest helium concentrations. The Rayleigh scattering pictures (Figure 2 through Figure 6) show that the helium outside of the vortex cores mixes faster than the helium inside the cores. Therefore, the cores quickly become coincident with the regions of highest helium concentrations. Figure 9 shows this spacing with increasing time. At early times the spacing increases as the helium moves away from the center line, and concentrates in the vortex cores. Even after the formation of well developed core regions, the spacing still appears to increase slowly, especially for the higher mach number cases. This behavior is typical of decaying vortex pairs.

Figure 9 clearly shows that as the Mach

number increases the spacing between the vortices also increases. This may be the result of the increased lateral compression of the shock wave. Since the vorticity distribution is initially more compact for a stronger shock, less relative motion occurs before the vortex cores form. One of the first induced motions of the vorticity spiral is a motion toward the center line. For lower Mach numbers, a wider spiral allows the vorticity to move further in this direction. At higher Mach numbers the tighter spiral ensures the vorticity stays further from the centerline.

Also, as the shock Mach number increases, the jet cross-section deforms faster. In the limit of acoustic waves, the entire interaction occurs before any deformation of the cross section occurs. At higher Mach numbers the fluids behind the shock move at a significant fraction of the shock wave velocity, and the cross section starts to deform before the incident shock passes all the way through the jet. For weaker shocks, the vorticity on the downstream side of the cross section induces a motion on the upstream side toward the symmetry line of the structure. For stronger shocks, the vortex pair starts to form before this vorticity on the downstream side is created. As a result the vortex roles up further from the symmetry line and the spacing between the cores is larger.

Other trends are also visible in Figure 9. Decreasing the Atwood number increases the spacing between the vortex cores. Furthermore, after the reflected shock, the regions of highest helium concentration coincide with the strong inner vortex cores. These vortices are closer together than the vortex pair before the reflected shock interaction. Figure 9 confirms this, as the spacing decreases after the reflected shock.

3.3 Comparison with Previous Studies.

3.3.1 Vortex Pair Velocity and Spacing

Figure 10 and Figure 11 compare the velocity and spacing of the current experiments with the results of Yang (1994b) and Jacobs (1992) as functions of Mach number and Atwood number. To be consistent with Yang (1994b), the velocity and spacing are based on the center of mass-fraction defined as:

$$x_{cmf} = \frac{\iint_S fxdS}{\iint_S fdS}, \text{ and } y_{cmf} = \frac{\iint_S fydS}{\iint_S fdS},$$

where f is the mass-fraction, and S is the area. Jacobs (1992) based his values on the centroid of the region where the light intensity was above 50% of maximum intensity. The velocity is measured relative to the velocity of the ambient gas, and the spacing is an average value after well defined vortex cores have formed.

The cases that Yang (1994b) studied were very similar to but not exactly the same as the current experiments. Yang looked at cases with pure helium, 75% helium, 50% helium and 25% helium initially in the jet center, while the experiments had 92% and 43% helium. Also Yang mostly used a shock tube 8 jet diameters wide, with only a few simulations at different widths. For the experiments the shock tube was 25 jet diameters wide. Also, the width of the jet interface thickness in the experiments more closely matched the most diffuse case that Yang studied. However, only one simulation with this thickness was computed.

Therefore, the computational values were corrected for these differences. Interpolation was used to match density ratios. Corrections for channel spacing and interface thickness were based on scaling factors found from the cases that best matched the experimental conditions.

Experimentally, the velocity of the helium relative to the surrounding air is found by subtracting the air velocity calculated from the one dimensional, ideal gas, shock equations. At late times, after the formation of the vortex pair these velocities were nearly constant. It should be noted that this measurement is very sensitive to small errors in the measurement of the experimental Mach number. For example, for a Mach number close to one, the jump in velocity across the shock is proportional to *(M-1)*. In addition it is found that the velocity of the vortex pair is on the order of 10% of the jump in velocity across the shock. For a Mach 1.1 shock this implies that a 1% error in the Mach number would generate a 10% error in the calculated velocity behind the shock, and would cause a 100% error in the relative velocity of the vortex pairs. For the present experiments, the velocities were estimated to be known within 10%.

Figure 10a and b show very good agreement between the current experimental velocities and those

of the previous studies. The velocity of the center of mass-fraction continuously increases with increasing Mach number. However there is a knee in the curve near M=1.25, above which this increase falls off. Also, the velocity increases nearly linearly with Atwood number. The curve is expected to pass through the origin, which indicates the experimental result for an Atwood number of 0.22 is probably high. For this Atwood number (visualized in Figure 6), only the last few pictures were taken after the formation of well defined vortex pairs. As a result the measured velocity for that case is more susceptible to errors.

Figure 11 shows the vertical distance between the center of mass-fraction above and below the symmetry line; the distance is normalized by the initial jet diameter. Once again good agreement is found between the current experiments and Yang's computations. The results follow the same trends as the vortex spacing found from the regions of highest helium concentrations and shown in Figure 9. There is a slight increase of spacing with Mach number and a slight decrease with Atwood number.

Also shown is a model developed by Yang (1994b):

$$\bar{y}_\infty = \frac{\gamma_1}{2}(1+\frac{\rho_l}{\rho_h})$$

where $\bar{y}_\infty$ is the spacing normalized by the diameter after well developed vortex cores have formed, and γ_1 is the specific heat ratio of the ambient gas. The model agrees with the experiments and computations for low Mach numbers, and accounts for the variation with Atwood number. However, a variation with Mach number is not included, and differences occur with the computations and experiments for higher Mach numbers.

Figure 10 also shows poor agreement between Jacobs' spacing and those of the current experiments. This discrepancy is most likely due to a difference in the measurement of the initial jet diameter. The current Rayleigh Scattering technique measured Jacobs' jet diameter to be 0.90 cm, which is 36% larger than the diameter measured by the PLIF technique (0.66 cm). This affects the points in Figure 10 since the spacing is normalized by this diameter. Jacobs' experiments agree with the current ones if they are normalized by the value measured with the Rayleigh scattering technique.

It should be noted that the PLIF system did not view the helium directly, but instead measured

the diameter of the biacetyl tracer gas that was pre-mixed with the helium. Because biacetyl has a molecular weight of 86, it diffuses much slower than helium. In the initial laminar jet, the biacetyl has a smaller diameter since it tends to stay in the jet center, while the helium diffuses radially.

3.3.2 Circulation of the vortex cores.

The previous studies developed models for the magnitude of the circulation generated on either side of the symmetry line. Picone & Boris (1987) integrated the vorticity equation assuming a planar shock and found that:

$$\frac{\Gamma}{Da_1} = \frac{\Delta u}{a_1}\left(1 - \frac{\Delta u}{2a_1}\right)\ln\left(\frac{\rho_h}{\rho_l}\right),$$

where Γ is the magnitude of the circulation in the upper half plane, D is the initial jet diameter, a_l is the speed of sound in the ambient fluid, and Δu is the change in velocity across the shock traveling in the ambient fluid. Jacobs (1992) used the model of Rudinger & Somers to predict:

$$\frac{\Gamma}{Da_1} = A\frac{\Delta u}{a_1}.$$

Yang (1994b) used the vorticity equation, a similarity argument, and intuition to develop a model that can be rewritten in the form:

$$\frac{\Gamma}{Da_1} = 2A\frac{\Delta u}{a_1}\frac{\rho_1}{\rho_2},$$

where ρ_1 and ρ_2 are the densities of the ambient gas before and after the incident shock.

Although the circulation can not be measured directly in the experiments, it can be estimated from the Rayleigh scattering pictures. Yang's simulations show that most of the vorticity generated by the shock coalesces in the vortex pair, and very little of the vorticity is in the tail regions. This indicates that the total circulation generated by the shock interaction can be estimated using the formula for a point vortex pair: $\Gamma = 2\pi U_v y_v$, where U_v is the velocity of the vortex pair relative to the ambient fluid, and y_v is the distance between the point vortices. As in Figure 9 the vortex centers are assumed to be where the highest helium concentrations are. This estimate does not include the effect of the vortex core size which Yang (1994a) and Pierrehumbert (1980) have shown reduces the total induced velocity for the same total circulation.

Figure 12 shows the circulation for the models developed by Yang, Picone & Boris, and Rudinger & Somers, along with the estimates for the current experiments and the measured values for

Yang's simulations. Given the approximate nature of both the experimental estimates, and the similarity argument used by Yang (1994b), there is very good agreement between Yang's simulations, his model, and the current experiments. The Models of Picone & Boris, and Rudinger & Somers fail to predict the circulation.

As with the velocity measurements, the circulation continuously increases with Mach number, and there is a knee in the curve near *M=1.25*. This similarity between circulation and velocity reflects the slow change of the vortex spacing with Mach number. One interpretation of the knee in the curve recognizes that the circulation is the integral of the vorticity over area. Given Yang's similarity argument and the functional form of his circulation model, the vorticity may increase proportionally with the change in velocity across the shock, but the area decreases with ρ_1/ρ_2 do to the shock compression. For low Mach numbers ρ_1/ρ_2 is near one, and the circulation increases rapidly; as the Mach number increases the compression becomes more pronounced and limits the circulation increase. Also as predicted in Yang's model, the circulation varies linearly with the Atwood number.

3.4 Other Properties of the Vortex Pairs.

Shown in Table 1 are values of the Reynolds number of the vortex pairs defined as Γ/ν_2 and values of U_V/a_2 which give an indication of the effect compressibility on the vortex pair.

Table 1

Mach #/P_1(atm)	Γ/ν_2	U/a_2
1.07/1.0	2800	0.02
1.14/0.55	3990	0.037
1.50/0.23	4900	0.058
2.00/0.08	2450	0.054

Here, ν_2 and a_2 are the kinematic viscosity and speed of sound after the shock interaction. Although the values of Γ/ν_2 are as high as 5000, the vortex pairs appear laminar in the pictures of the cross sections viewed by planar Rayleigh scattering and the shadowgraph pictures in Jacobs (1992), and Budzinski (1992). It should be noted that the stratification of the light helium in the centers of the vortex cores and the heavy air outside the cores helps to stabilize the flow. Yang (1991) used the results of Moore and Pullin (1987) to show that the velocity of

the vortex pairs is not significantly affected by compressibility for values of U_V/a_2 below 0.06. Therefore, compressibility does not play an important role in the current experiments.

Acknowledgement
AFOSR thanks Dr J Tishkoff

4. Conclusions

Planar laser Rayleigh scattering was used to experimentally study the deformation and motion of a laminar jet of helium in air after a shock interaction. The shock Mach number and gas Atwood number were varied, and the effect of a reflected shock was studied.

After a shock interaction with a laminar jet of helium, the jet cross section distorts and moves relative to the surrounding air. The cross section is transformed into a vortex pair and tail regions from the baroclinically generated vorticity. As the shock Mach number increases the size of the tails decrease. After a reflected shock interaction, each vortex core is split into an inner region of vorticity and an outer region of vorticity. The inner region is of the same sign as the original vortex core, and is stronger than the outer vortex which is of the opposite sign to the original. Vorticity is also generated in the pre reflected shock tail regions, and for a Mach 2.0 interaction, this vorticity is wrapped around the strong inner vortex cores.

After an incident shock interaction, the circulation of the vortices and the velocity of the helium center of mass-fraction continuously increase with increasing Mach number. However there is a knee in the curves near M=1.25, above which this increase falls off. Also, the velocity and circulation increase nearly linearly with Atwood number. The spacing between the vortex cores increases slightly with Mach number and decreases slightly with Atwood number.

~~Very~~ Good qualitative and quantitative agreement is found with Yang's previous simulations and models.

5. References

Budzinski, J. M. 1992 Planar Rayleigh scattering measurements of shock enhanced mixing. Ph. D. Thesis California Institute of Technology.

Budzinski, J. M. 1992 Rayleigh Scattering Measurements of Shock Enhanced Mixing. *AIAA Paper 92-3546*

Budzinski, J. M., Zukoski, E. E., Marble, F. E. 1995 The mixing after shock interactions with laminar jets of helium. To be submitted to Phys. Fluids.

Drummond, J. P., Carpenter, M. H., Reggins, D. W., and Adams, M. S. 1989 Mixing enhancement in a supersonic combustor. *AIAA Paper 89-2794.*

Eckbreth, A. C. 1988 Laser diagnostics for combustion temperature and species, Abacus Press, Tunbridge Wells, Kent.

Haas, J. L. 1984 Interaction of weak shock waves and discrete gas inhomogeneities. Ph.D. Thesis, California Institute of Technology.

Haas, F., and Sturtevant, B. 1987 Interaction of weak shock waves with cylindrical and spherical gas inhomogeneities. *J. Fluid Mech.* **181**, 41-76.

Jacobs, J. W. 1992 Shock-induced mixing of a light-gas cylinder. *J. Fluid Mech.* **234**, 629-649.

Jacobs, J.W. 1993 The dynamics of shock accelerated light and heavy gas cylinders. Phys. Fluids A **5**, 2239-2247.

Liepmann, H. W., Roshko, A., Coles, D., and Sturtevant, B. 1962 A 17-inch diameter shock tube for studies in rarefied gas dynamics. *Rev. Sci. Instrum.* **33**, 625-631.

Marble, F. E., Hendricks, G. J., and Zukoski, E. E. 1987 Progress toward shock enhancement of supersonic combustion processes. *AIAA Paper 87-1880.*

Marble, F. E., Zukoski, E. E., Jacobs, J. W., Hendricks, G. J., and Waitz, I. A. 1990 Shock enhancement and control of hypersonic mixing and combustion. *AIAA Paper 90-1981.*

Meshkov, E. E. 1969 Instability of the interface of two gasses accelerate by a shock wave. *Izv. Akad. Nauk. SSSR Mekh. Zhidk. Gaza* **4**, 151-157 [*Fluid Dyn.* **4**, 101-104]

Moore, D. W. and Pullin, D. I. 1987 The compressible vortex pair. *J. Fluid Mech.* **185**, 171-204.

Picone, J. M. and Boris, J. P. 1988 Vorticity generation by shock propagation through bubbles in a gas. *J. Fluid Mech.* **189**, 23-51.

Pierrehumbert, R. T. 1980 A family of steady, translating vortex pairs with distributed vorticity. *J. Fluid Mech.* **99**, 129-144.

Richtmyer, R. D. 1960 Taylor instability in shock acceleration of compressible fluids. *Commun. Pure Appl. Math.* **13**, 297-319.

Rudinger, G. and Somers, L. M. 1960 Behavior of small regions of different gases carried in accelerated gas flows. *J. Fluid Mech.* 7,. 161-176.

Samtaney, R., Zabusky, N. J. 1994 Circulation deposition on shock-accelerated planar and curved density-stratified interfaces: models and scaling laws. J. Fluid Mech.

Waitz, I. A. 1991 An investigation of contoured wall injectors for hypervelocity mixing augmentation. Ph.D. Thesis, California Institute of Technology.

Waitz, I. A., Marble, F. E., and Zukoski, E.E. 1991 An investigation of a contoured wall injector for hypervelocity mixing augmentation. *AIAA Paper 91-2265.*

Waitz, I. A., Marble, F. E., and Zukoski, E.E. 1992 A systematic experimental and computational investigation of a class of contoured wall fuel injectors. *AIAA Paper 92-0625.*

Yang, J. 1991 An analytical and computational investigation of shock-induced vortical flows with applications to supersonic combustion. Ph.D. Thesis, California Institute of Technology.

Yang, J., Kubota, T., Zukoski, E. E. 1993 Applications of shock-induced mixing to supersonic combustion. *AIAA J.* **5**, 854-862.

Yang, J., Kubota, T. 1994 The steady motion of a symmetric, finite core size, counterrotating vortex pair. *SIAM J. Appl. Math.* **54**, 14-25.

Yang, J., Kubota, T., Zukoski, E. E. 1994 A model for characterization of a vortex pair formed by shock passage over a light-gas inhomogeneity. *J. Fluid Mech.* **258**, 217-244.

Yang, X., Zabusky, N. J., 1990 "Breakthrough" via dipolar -vortex/jet formation in shock-accelerated density-stratified layers. Phys. Fluids A **2**, 892-895.

6. Figure Captions

Figure 1. Side view of the GALCIT 17 inch shock tube.

Figure 2. Rayleigh scattering pictures after a Mach 1.066 shock traveling in air interacts with a jet of helium. Initially, on the jet centerline the molar concentrations are 92% helium and 8% air. a) through h) are after an incident shock only. i) through *l*) are after both an incident and a reflected shock interaction. The first shock interaction occurs at t/τ=0, and the reflected shock interaction occurs at t/τ=29. Here, τ is the time scaling developed by Yang (1994), and $\tau = D/(8A\Delta u)$. A, the Atwood number, is equal to 0.66. Δu is the velocity jump across the shock in the air, and D is the initial jet diameter. In the above sequence, the times after the incident shock interaction are a) t/τ=0, b) 6.2, c) 17.9, d) 29.3, e) 45.1, f) 47.6, g) 54.8, h) 68.6, i) 35.6, j) 40.8, k) 46.4, l) 63.6.

Figure 3. Rayleigh scattering pictures after a Mach 1.14 shock interaction. The Atwood number is 0.66. a) through f) are after an incident shock only. g) through i) are after both an incident and a reflected shock interaction. The first shock interaction occurs at t/τ=0, and the reflected shock interaction occurs at t/τ=11.5. a) t/τ=0, b) 4.56, c) 16.6, d) 21.1, e) 30.8, f) 46.8, g) 50.3, h) 61.6, i) 69.2.

Figure 4. Rayleigh scattering pictures after a Mach 1.50 shock interaction. The Atwood number is 0.66. a) t/τ=11.4, b) 18.8, c) 27.7, d) 38.3, e) 46.9, f) 58.0. The shock is visible in a) as a transition from dark to light on the right side of the picture.

Figure 5. Rayleigh scattering pictures after a Mach 2.0 shock interaction. The Atwood number is 0.66. a) through g) are after an incident shock only. h) through k) are after both an incident and a reflected shock interaction. The first shock interaction occurs at t/τ=0, and the reflected shock interaction occurs at t/τ=77.6. a) t/τ=16.2, b) 24.8, c) 30.7, d) 34.7, e) 54.8, f) 68.0, g) 80.2, h) 77.6, i) 83.16, j) 88.8, k) 97.7. The incident shock is visible in pictures a, & b; the reflected shock is visible in pictures h, i, & j.

Figure 6: Rayleigh scattering pictures after a Mach 1.14 shock interaction. The Atwood number is 0.22. a) through f) are after an incident shock only. g) through i) are after both an incident and a reflected shock interaction. The first shock interaction occurs at t/τ=0, and the reflected shock interaction occurs at t/τ=11.5. a) t/τ=0, b) 4.81, c) 8.22, d) 11.04, e) 15.5, f) 20.1, g) 23.0, h) 29.2, i) 45.38, j) 20.5, k) 23.6, l) 25.7, m) 30.7, n) 35.4, o) 44.9. The incident shock is visible in picture a, and the reflected shock is visible in picture j.

Figure 7. Path of the vorticity that is generated near the top and bottom of the initially circular cross-section.

Figure 8. x-t diagram for the experiments.

Figure 9. Distance between the vortex cores. a) A=0.66, b) A=0.22

Figure 10. Velocity of the helium center of helium mass-fraction for the current experiments, Yang's (1994b) simulations, and Jacobs' (1992) experiments. a) with varying Mach number, b) with varying Atwood number.

Figure 11. Spacing between the center of helium mass-fractions above and below the symmetry line for the current experiments, Yang's (1994b) simulations, and Jacobs' (1992) experiments. a) with varying Mach number, b) with varying Atwood number.

Figure 12. Circulation for the current experiments, Yang's (1994b) simulations and model, the model of Picone & Boris (1988), and Rudinger & Somers (1960). a) with varying Mach number, b) with varying Atwood number.

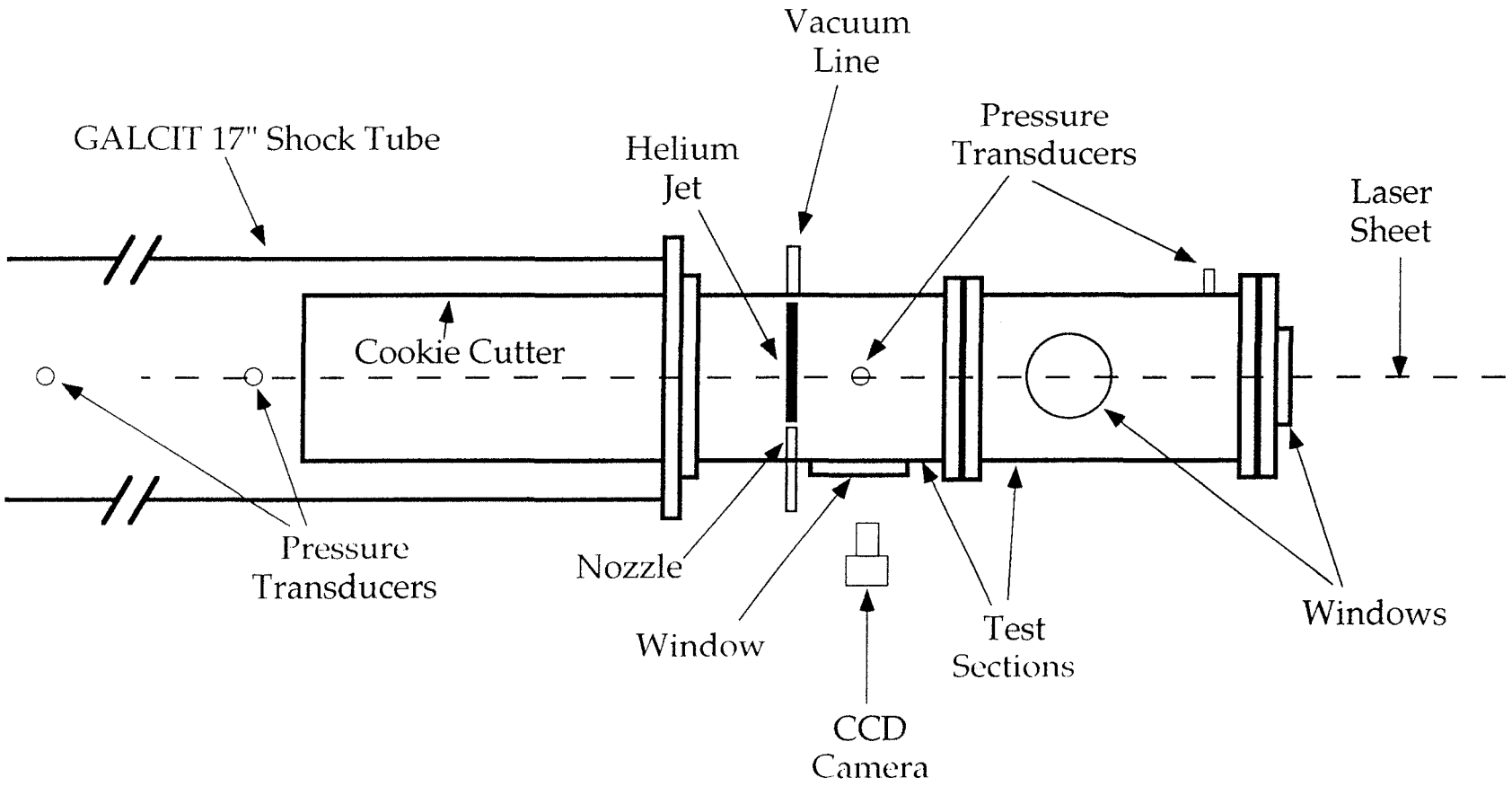
Vacuum
Line
GALCIT 17" Shock Tube
Helium
Jet
Pressure
Transducers
Laser
Sheet
Cookie Cutter
Pressure
Transducers
Nozzle
Window
CCD
Camera
Test
Sections
Windows

Figure 1.

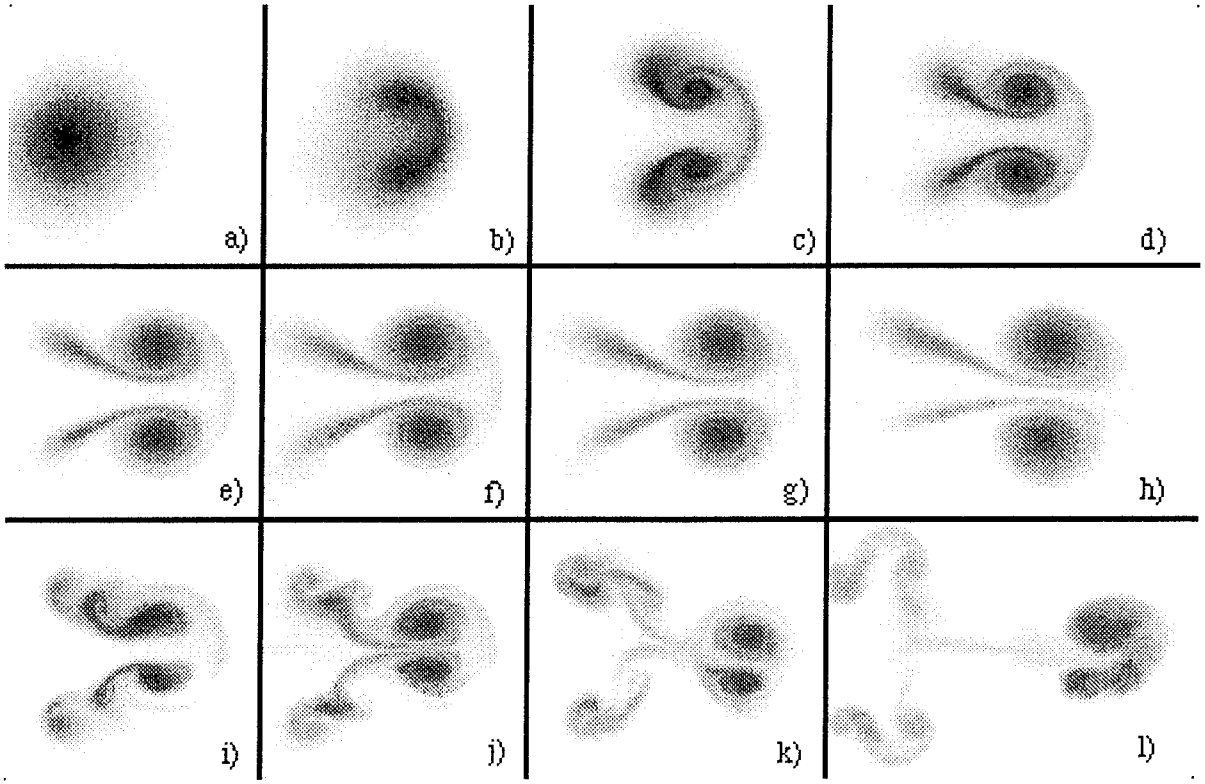

Figure 2.

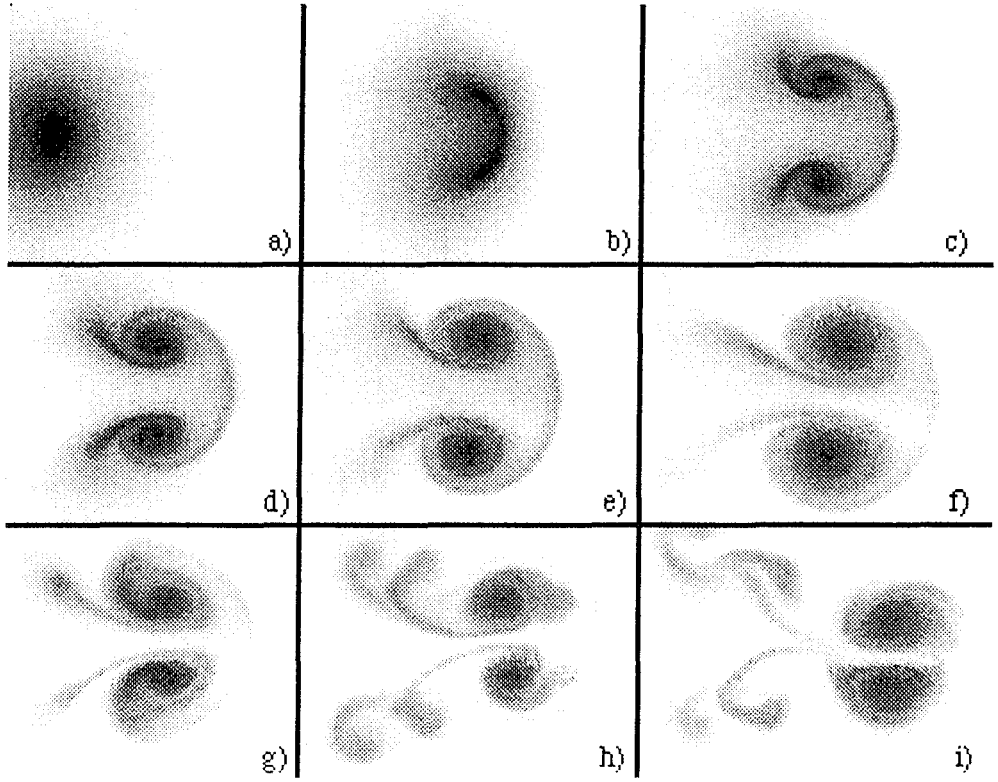

Figure 3.

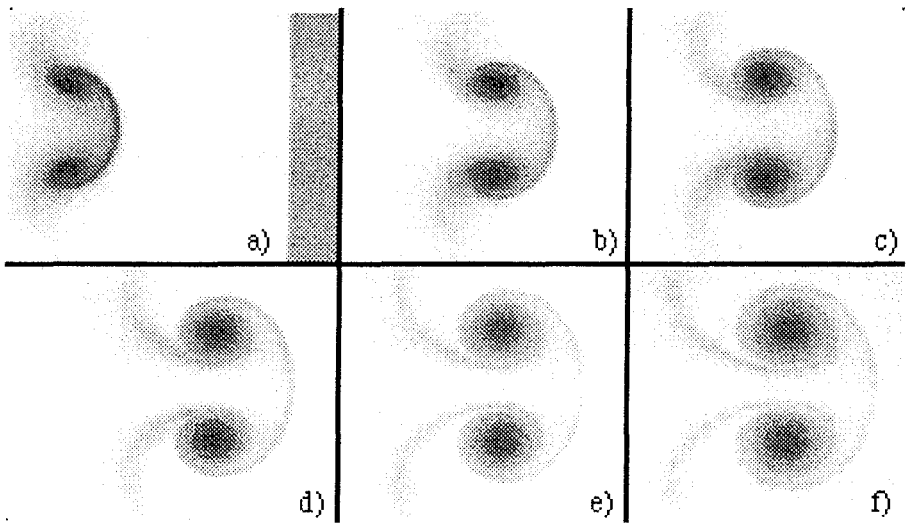

Figure 4.

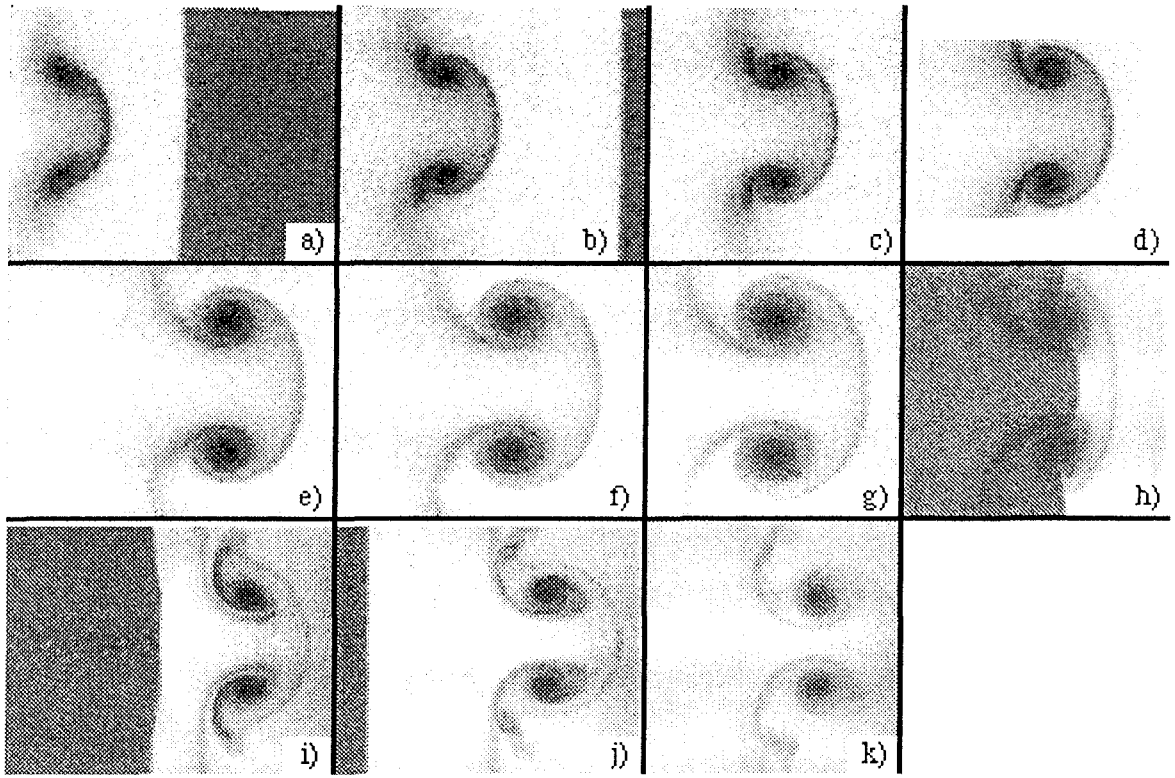

Figure 5.

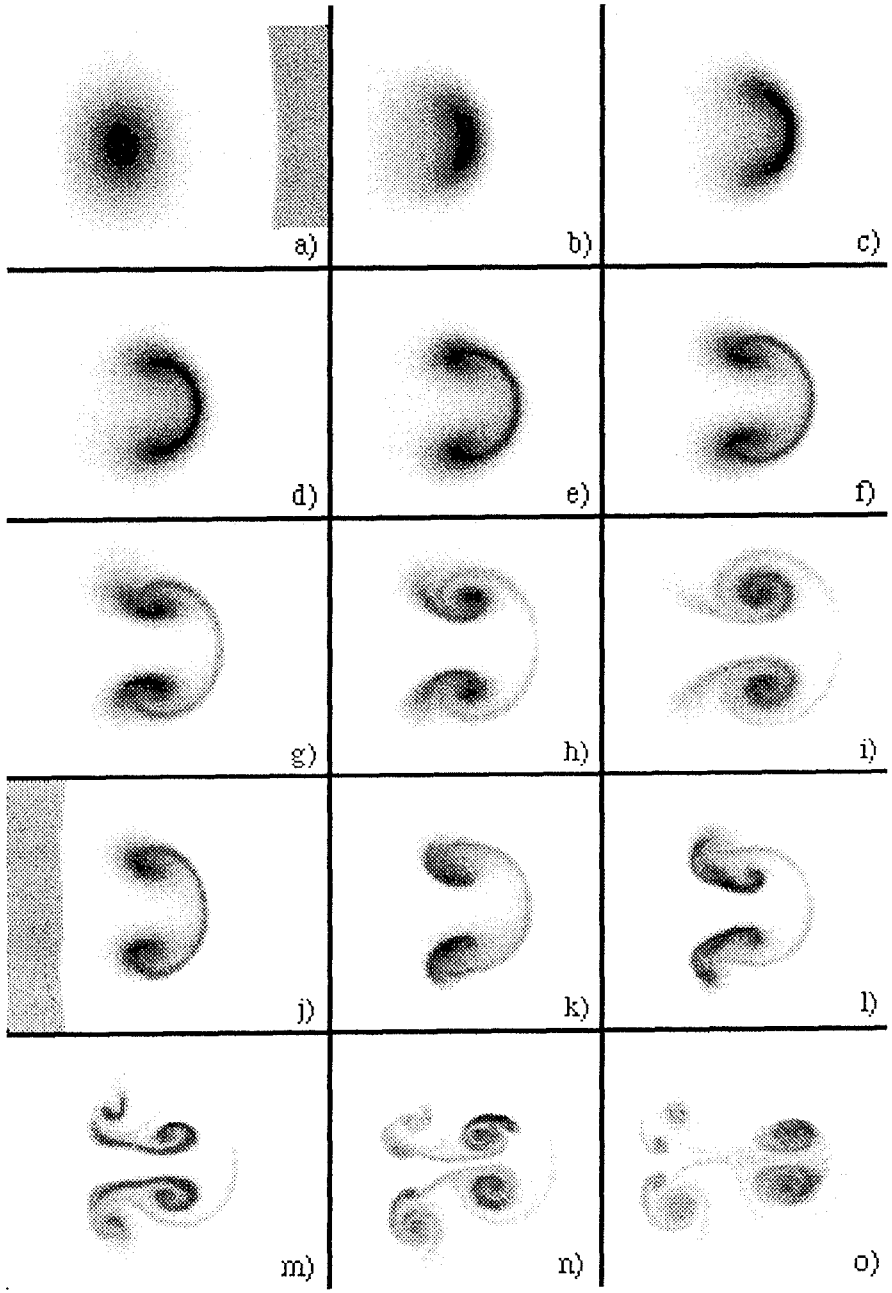

Figure 6.

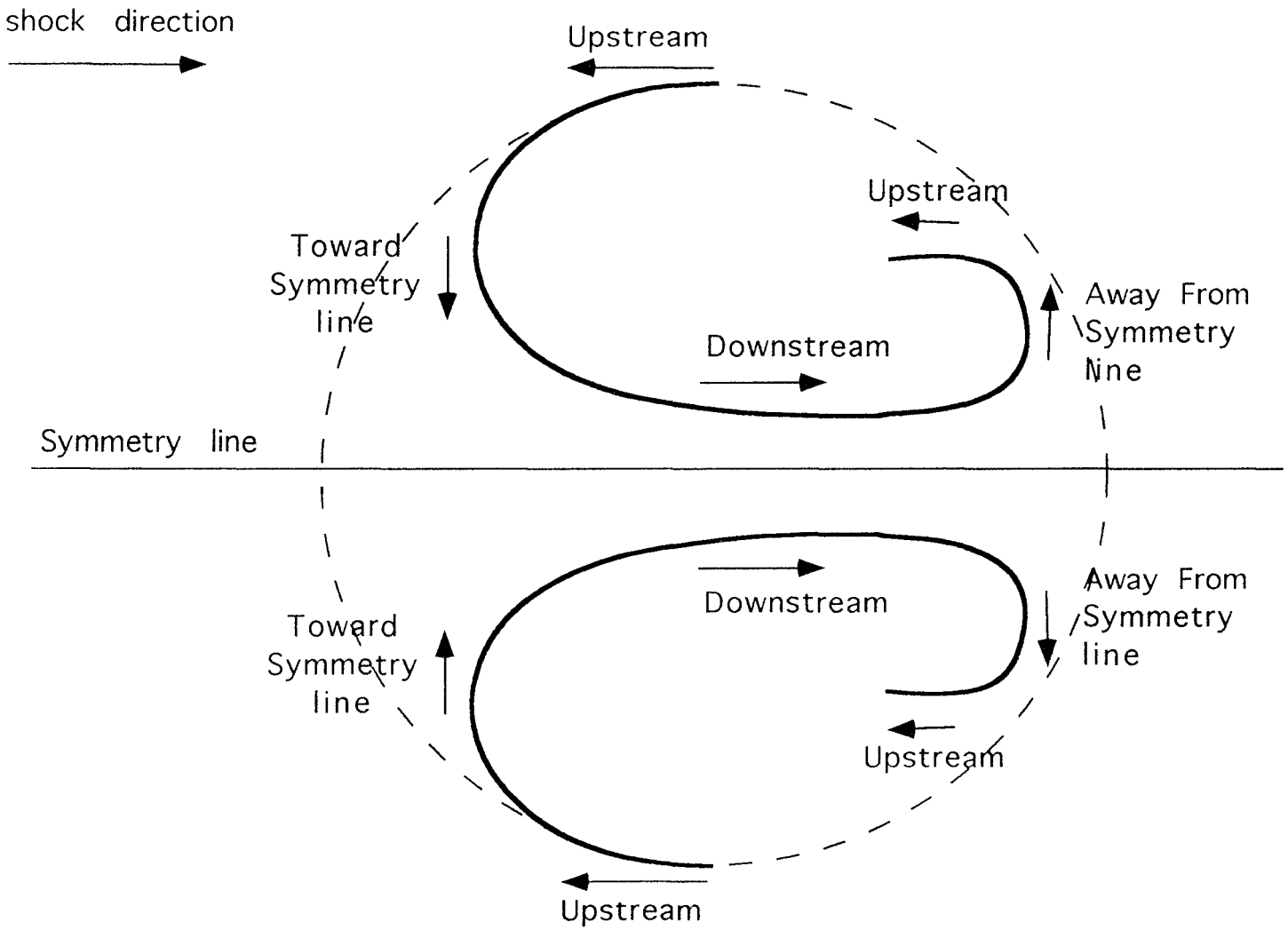
shock direction
Upstream
Upstream
Toward Symmetry line
Away From Symmetry line
Downstream
Symmetry line
Downstream
Away From Symmetry line
Toward Symmetry line
Upstream
Upstream

Figure 7.

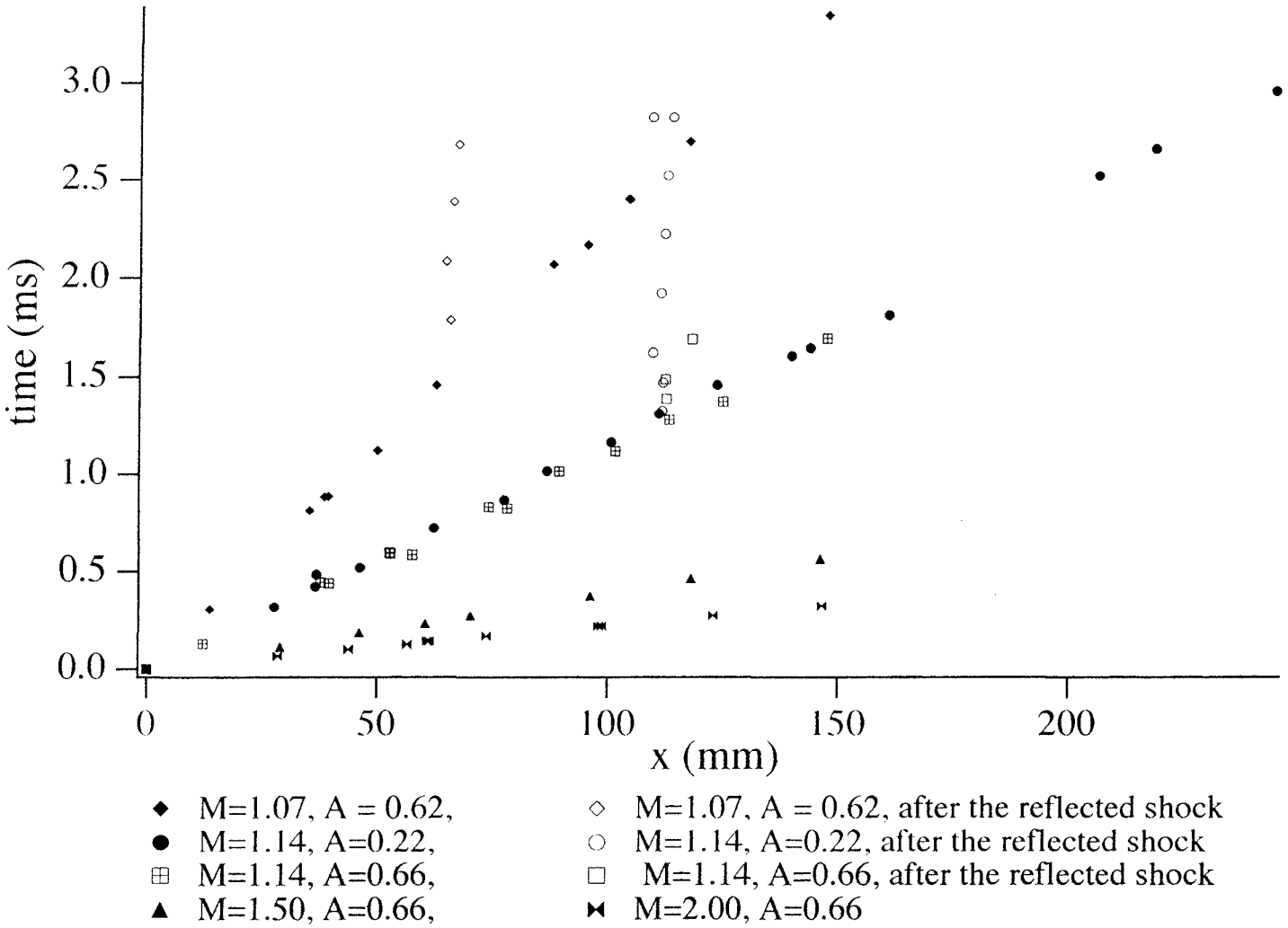
time (ms)
3.0
2.5
2.0
1.5
1.0
0.5
0.0
0
50
100
150
200
x (mm)
M=1.07, A = 0.62,
M=1.14, A=0.22,
M=1.14, A=0.66,
M=1.50, A=0.66,
M=1.07, A = 0.62, after the reflected shock
M=1.14, A=0.22, after the reflected shock
M=1.14, A=0.66, after the reflected shock
M=2.00, A=0.66

Figure 8.

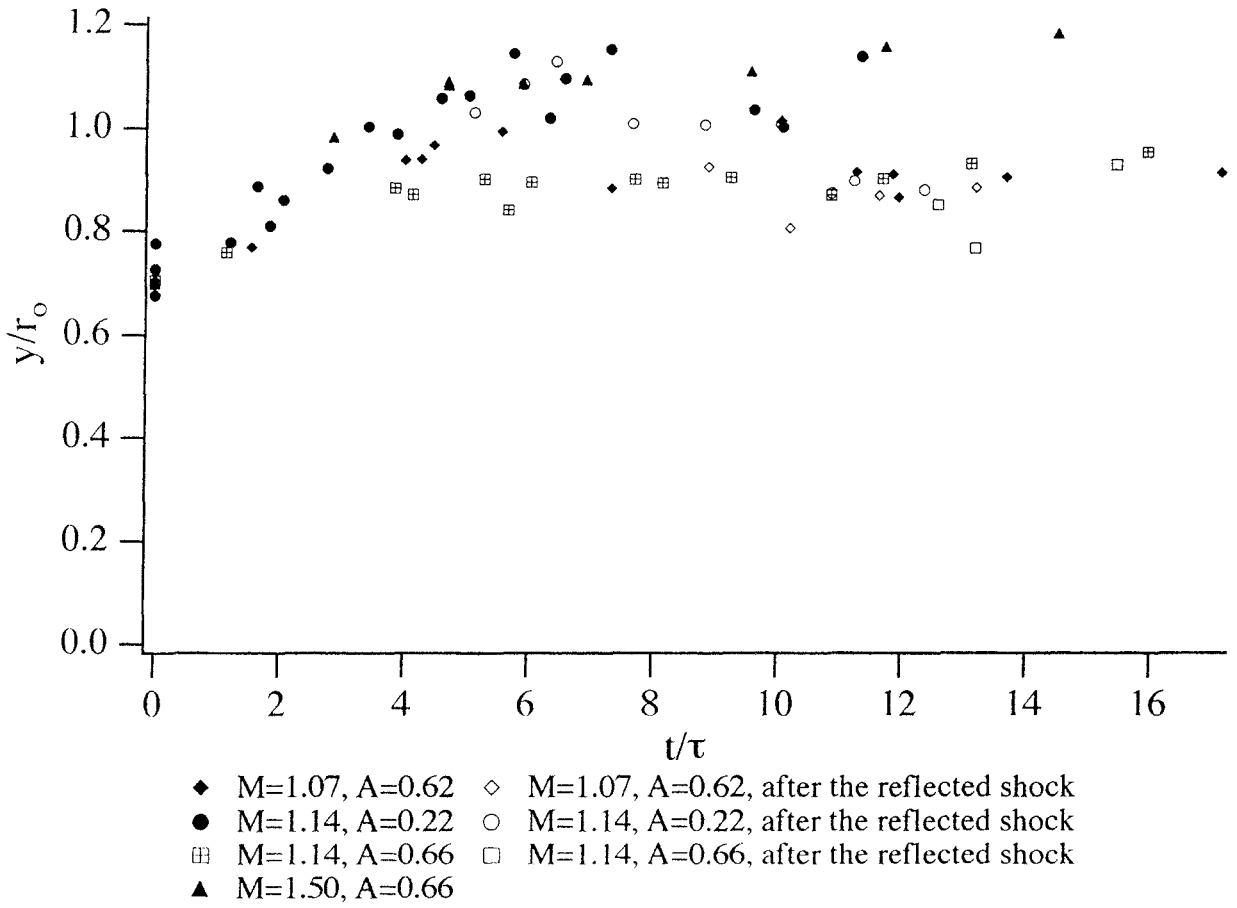
1.2
1.0
0.8
0.6
0.4
0.2
0.0
y/r_o
0
2
4
6
8
10
12
14
16
t/τ
M=1.07, A=0.62
M=1.07, A=0.62, after the reflected shock
M=1.14, A=0.22
M=1.14, A=0.22, after the reflected shock
M=1.14, A=0.66
M=1.14, A=0.66, after the reflected shock
M=1.50, A=0.66

Figure 9a.

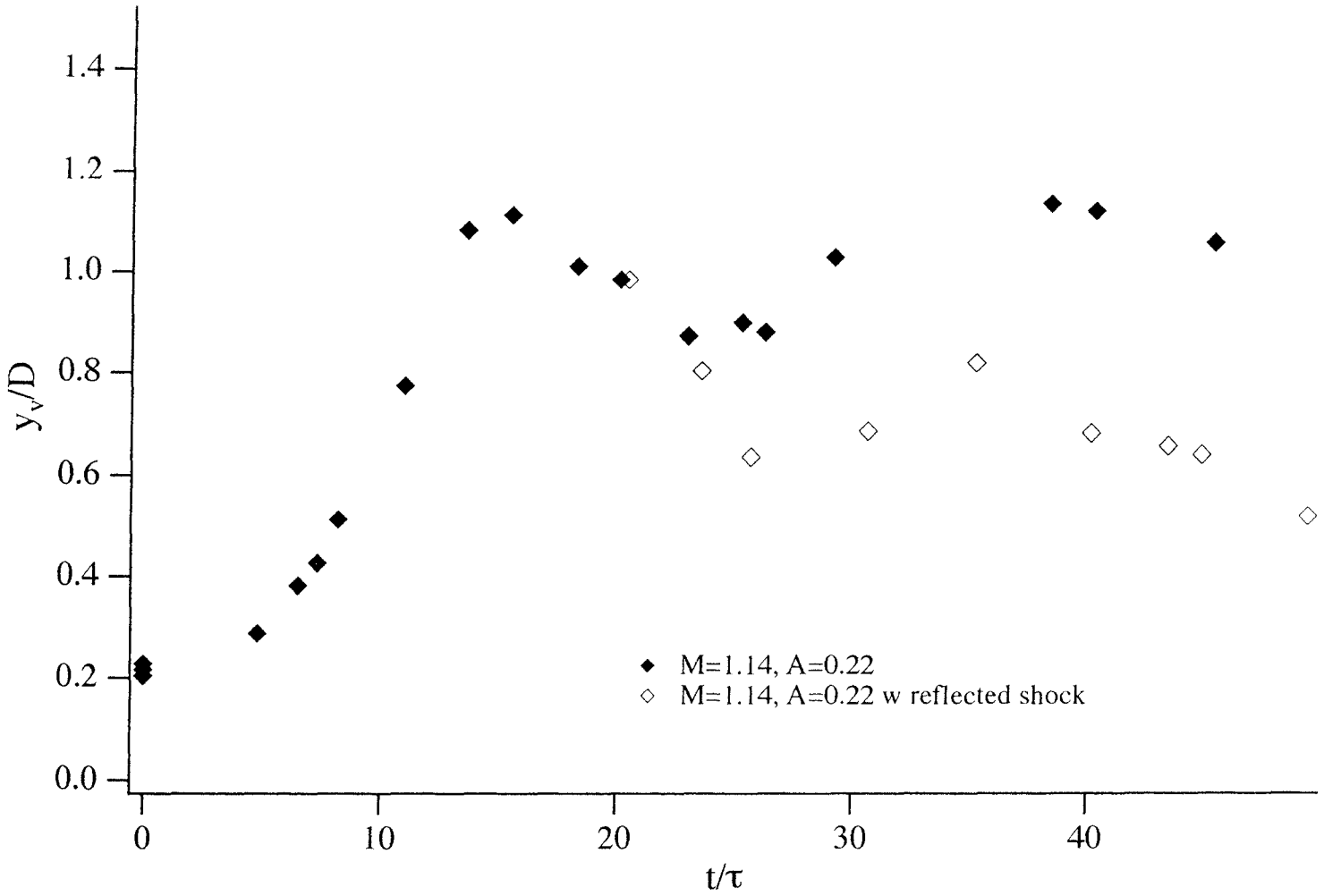
1.4
1.2
1.0
0.8
0.6
0.4
0.2
0.0
y_v/D
0
10
20
30
40
t/τ
M=1.14, A=0.22
M=1.14, A=0.22 w reflected shock

Figure 9b.

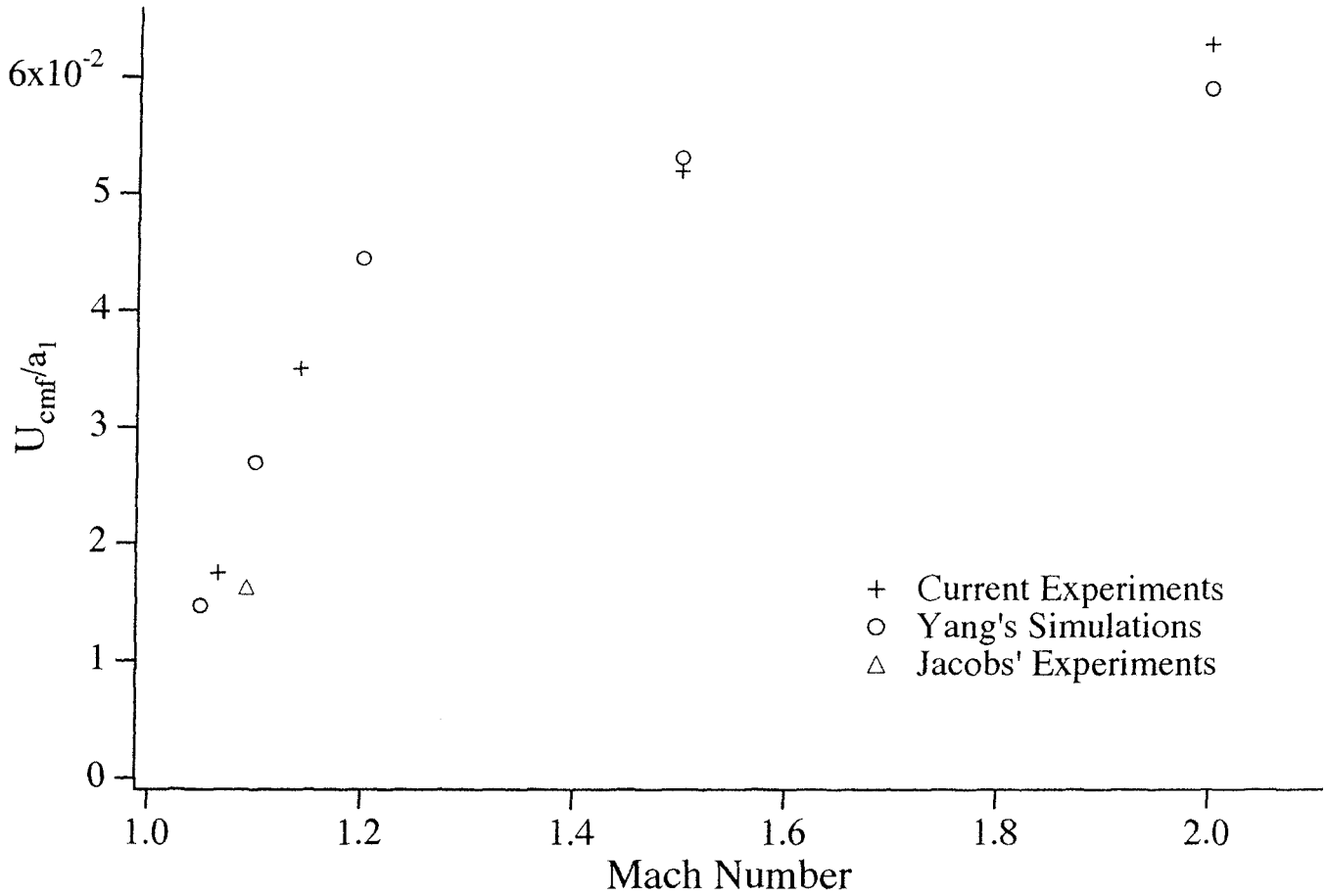
6x10-2
5
4
3
2
1
0
Ucmf/a1
1.0
1.2
1.4
1.6
1.8
2.0
Mach Number
+ Current Experiments
○ Yang's Simulations
△ Jacobs' Experiments

Figure 10a.

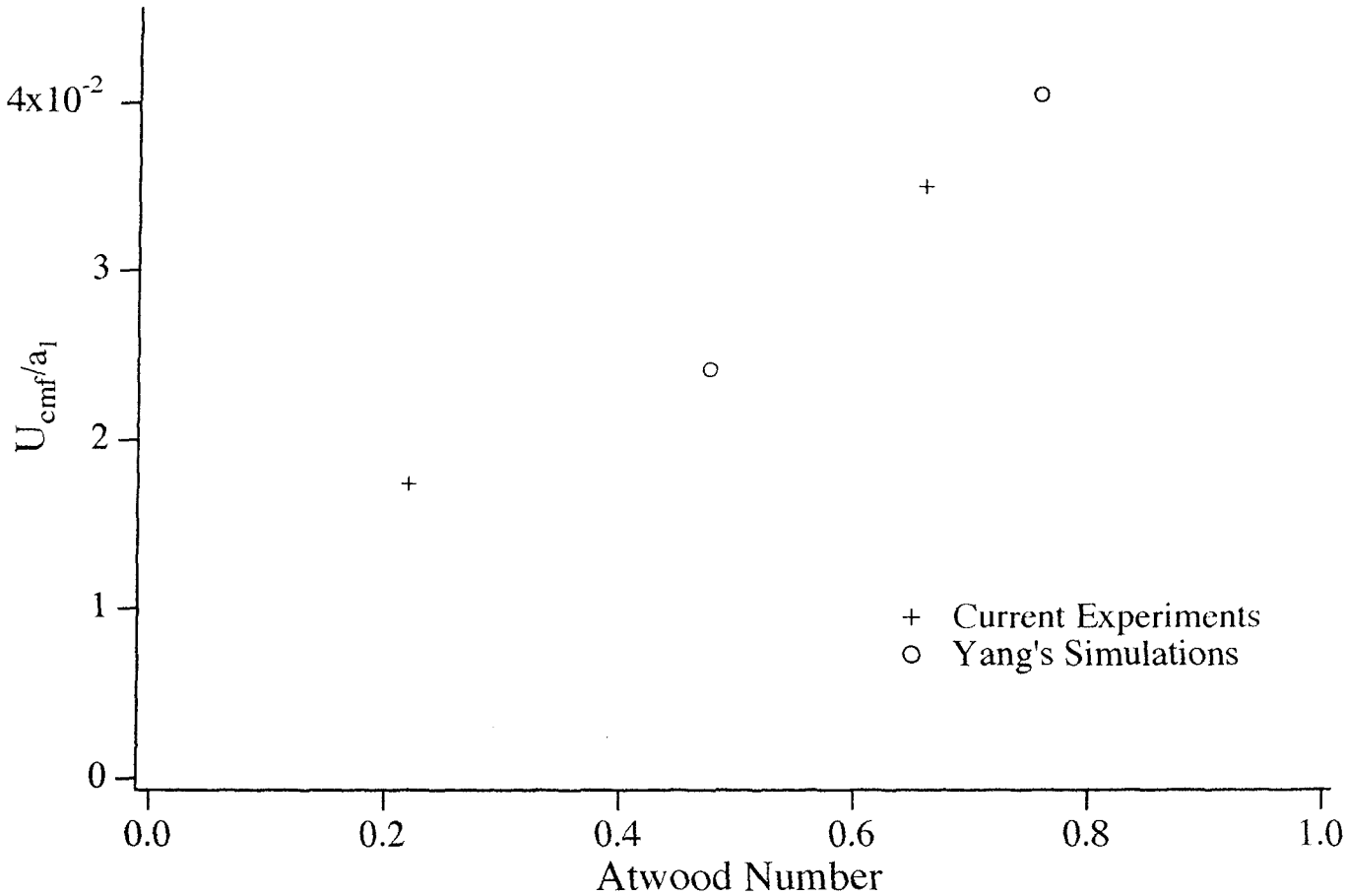
4x10-2
3
2
1
0
Ucmf/a1
0.0
0.2
0.4
0.6
0.8
1.0
Atwood Number
+ Current Experiments
o Yang's Simulations

Figure 10b.

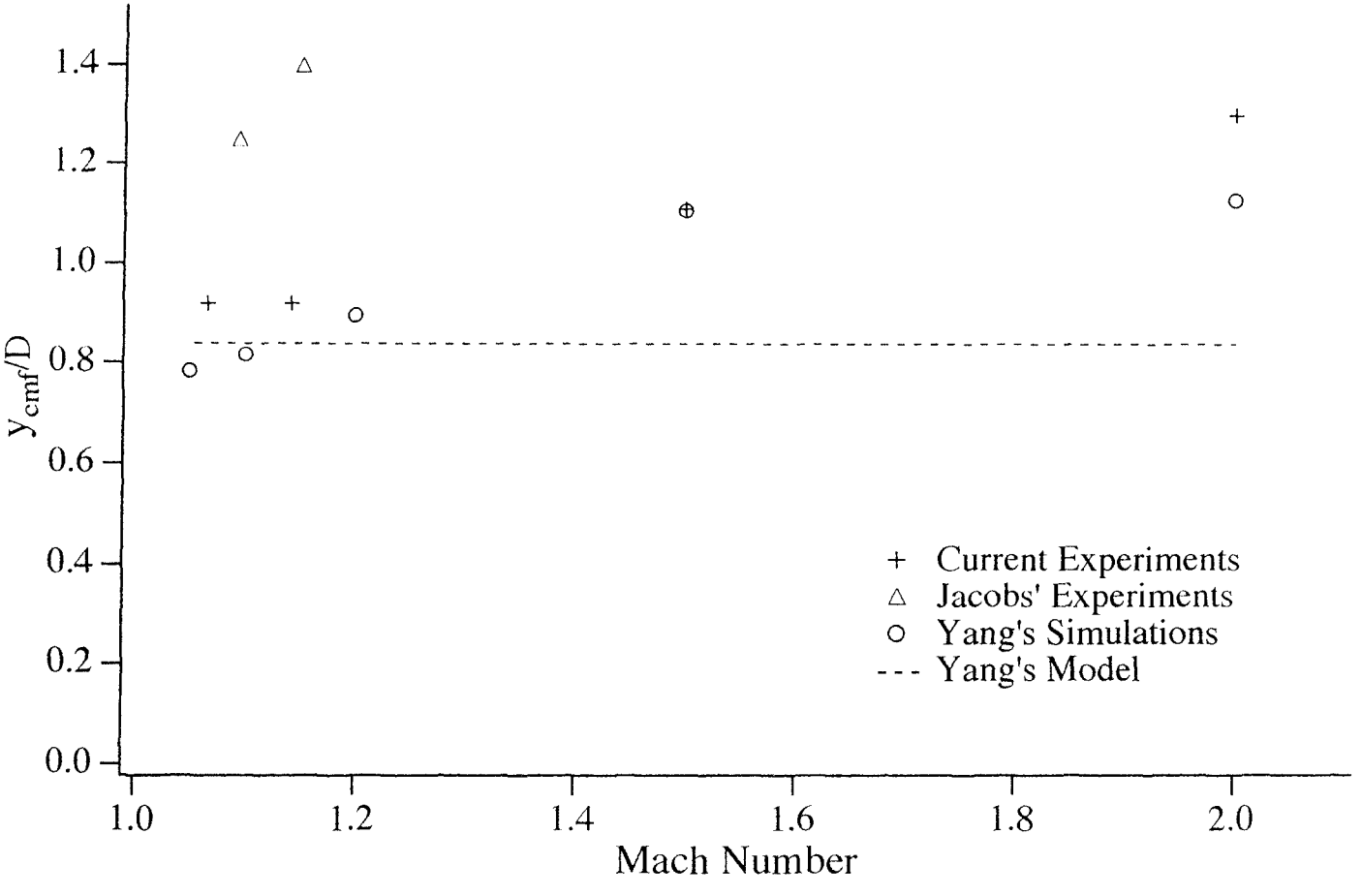
1.4
1.2
1.0
0.8
0.6
0.4
0.2
0.0
y_{cmf}/D
1.0
1.2
1.4
1.6
1.8
2.0
Mach Number
+ Current Experiments
△ Jacobs' Experiments
○ Yang's Simulations
--- Yang's Model

Figure 11a.

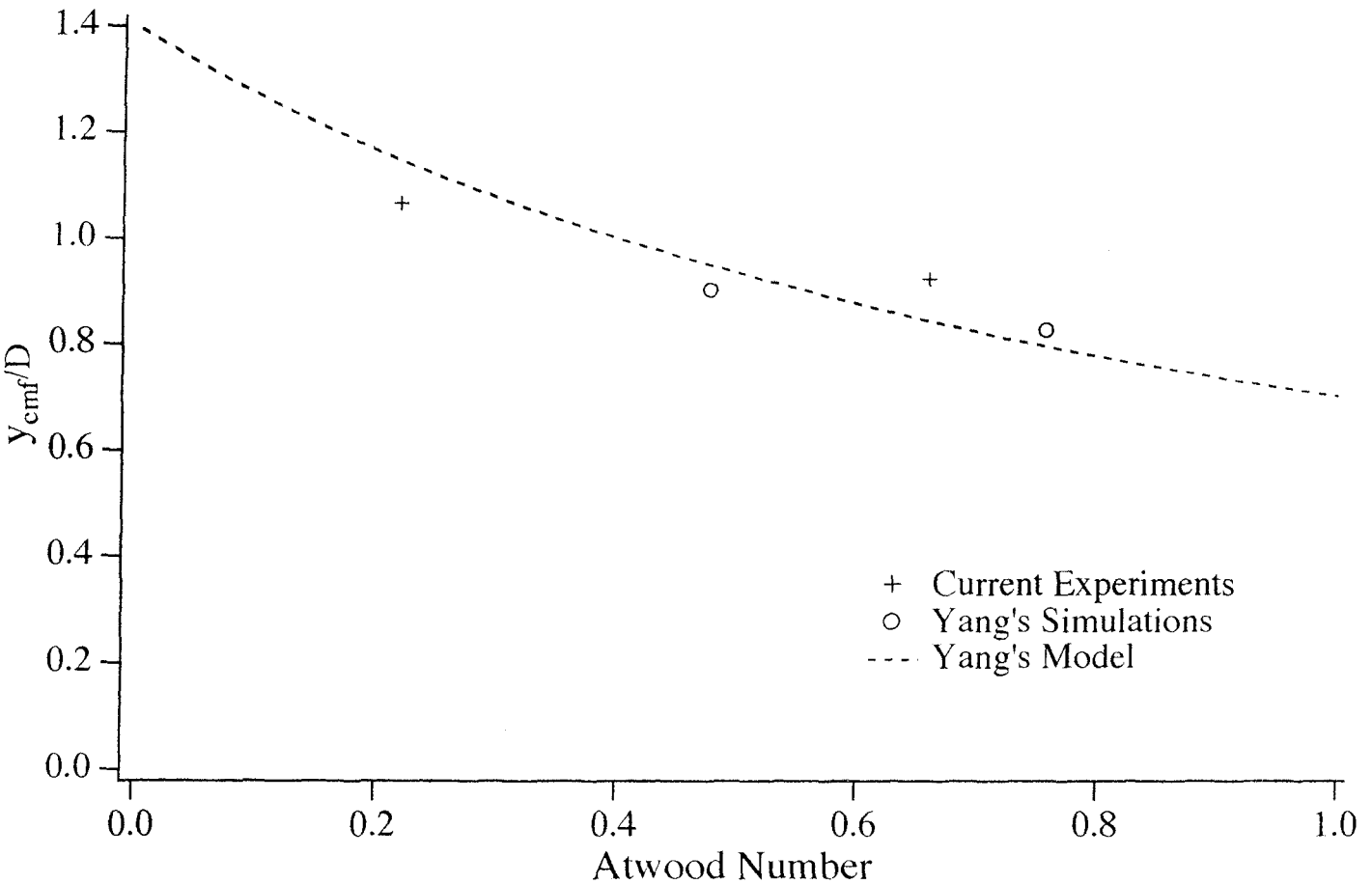
1.4
1.2
1.0
0.8
0.6
0.4
0.2
0.0
y_{cmf}/D
0.0
0.2
0.4
0.6
0.8
1.0
Atwood Number
+ Current Experiments
○ Yang's Simulations
--- Yang's Model

Figure 11b.

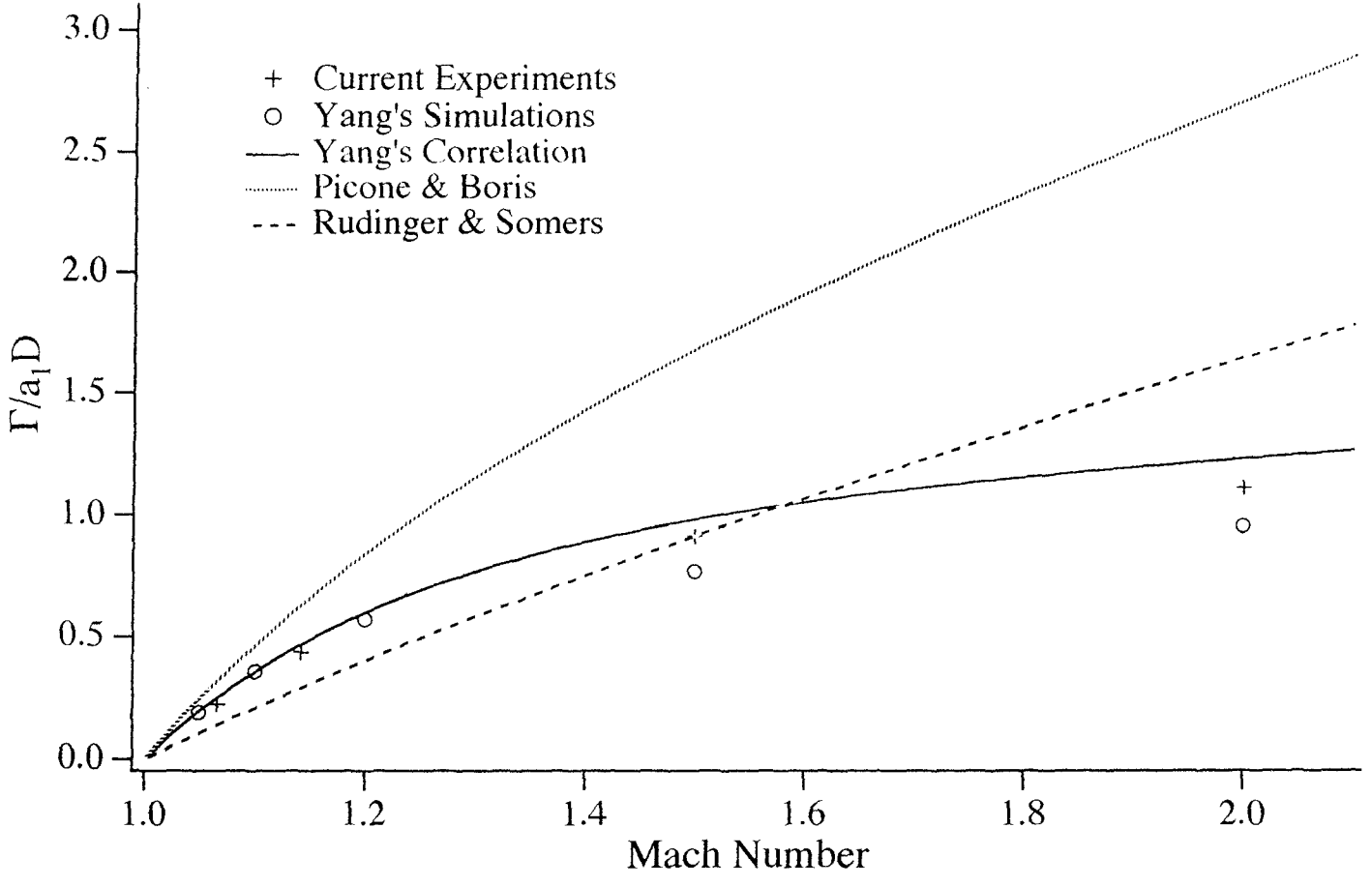
3.0
2.5
2.0
1.5
1.0
0.5
0.0
Γ/a1D
+ Current Experiments
○ Yang's Simulations
Yang's Correlation
Picone & Boris
Rudinger & Somers
1.0
1.2
1.4
1.6
1.8
2.0
Mach Number

Figure 12a.

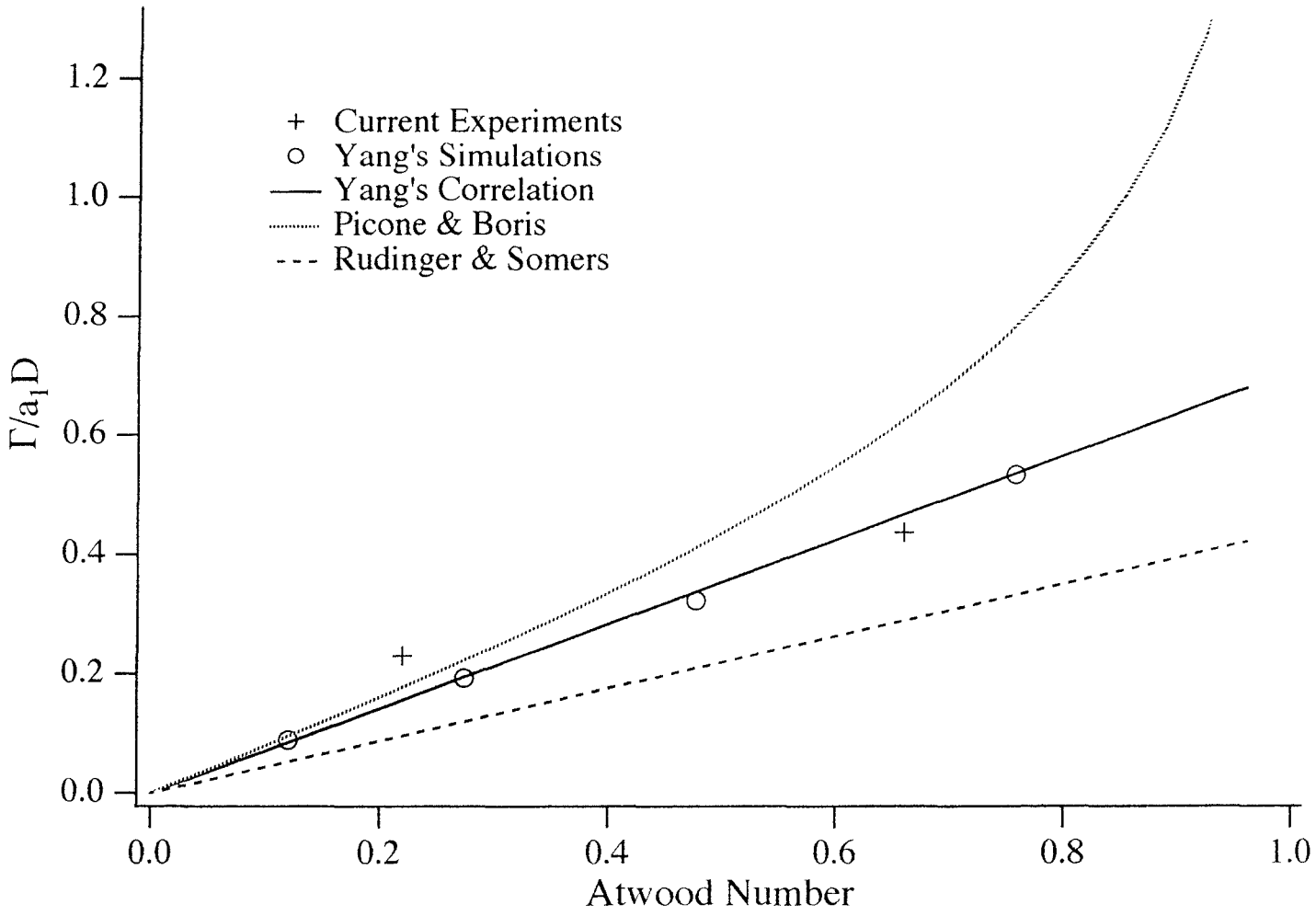
+ Current Experiments
o Yang's Simulations
Yang's Correlation
Picone & Boris
Rudinger & Somers
Γ/a1D
1.2
1.0
0.8
0.6
0.4
0.2
0.0
0.0
0.2
0.4
0.6
0.8
1.0
Atwood Number

Figure 12b.